JOURNAL OF SPACECRAFT AND ROCKETS
Vol. 47, No. 2, March–April 2010

# Electrodynamic Tethers Under Forced-Current Variations Part 2: Flexible-Tether Estimation and Control

Paul Williams*
*Delft University of Technology, 2629 HS Delft, The Netherlands*

DOI: 10.2514/1.45733

**The dynamic estimation of the state of an electrodynamic tether system is considered for the purposes of feedback control. A filter is developed based on an inelastic tether model, which is used to estimate the tether libration dynamics. This is coupled with an energy-rate feedback-control scheme for tracking a desired libration trajectory. A filter is also developed that takes into account the effects of tether flexibility. Only measurements of the tether-end body position and the tension vector at the main spacecraft are required to estimate the tether shape and libration dynamics. A square-root implementation of an unscented filter is used to robustly estimate the tether dynamic state using a discretized tether model. A modified energy-rate feedback controller is proposed taking into account the lateral oscillations of the tether. Numerical results show that feedback of the tether-end body is insufficient for stabilizing a flexible tether. Results of simulations of the operation of the coupled estimation and control technique demonstrate that it is capable of stabilizing the librations and lateral oscillations of an electrodynamic tether.**

## Nomenclature

| | | |
|---|---|---|
| $\boldsymbol{B}$ | = | magnetic field vector |
| $E$ | = | nondimensional energy flux |
| $\mathcal{E}$ | = | nondimensional energy flux of tether tangent |
| $I$ | = | electric current, A |
| $i$ | = | orbit inclination, deg |
| $\mathcal{K}$ | = | Kalman gain |
| $k_1$ | = | feedback gain for tether librations |
| $k_2$ | = | feedback gain for lateral tether oscillations |
| $L$ | = | state dimension in unscented filter |
| $l_j$ | = | length of $j$th tether element, m |
| $m_j$ | = | mass of $j$th tether element, kg |
| $m_s$ | = | subsatellite mass, kg |
| $m_t$ | = | tether mass, kg |
| $n$ | = | number of tether elements |
| $\boldsymbol{Q}$ | = | process noise covariance |
| $R$ | = | orbit radius, m |
| $\boldsymbol{R}$ | = | measurement noise covariance |
| $\boldsymbol{S}$ | = | Cholesky form of covariance |
| $T$ | = | tether tension, N |
| $t$ | = | dimensional time, s |
| $\boldsymbol{u}$ | = | control input vector |
| $\boldsymbol{v}$ | = | process noise vector |
| $W$ | = | weights used in unscented filter |
| $\boldsymbol{w}$ | = | measurement noise vector |
| $\boldsymbol{x}$ | = | state vector |
| $\boldsymbol{y}$ | = | output measurement vector |
| $\varepsilon$ | = | amplitude of nondimensional current |
| $\bar{\varepsilon}$ | = | nondimensional current $f_e I \mu_m / \mu (m_s + m_t/3)$ |
| $\theta$ | = | in-plane libration angle, deg |
| $\Lambda_j$ | = | nondimensional length of $j$th tether element |
| $\mu$ | = | Earth's gravitational parameter, $m^3/s^2$ |
| $\mu_m$ | = | magnetic field dipole strength |
| $\nu$ | = | true anomaly, rad |
| $\tau$ | = | computational domain used in pseudospectral method |
| $\phi$ | = | out-of-plane libration angle, deg |
| $\mathcal{X}$ | = | sigma points |
| $\Omega$ | = | longitude of ascending node, deg |
| $\omega$ | = | orbital angular velocity, rad/s |
| $\varpi$ | = | argument of perigee, deg |

*Subscript*

| | | |
|---|---|---|
| ref | = | reference periodic solution |

*Superscripts*

| | | |
|---|---|---|
| $'$ | = | $\mathrm{d}/\mathrm{d}(\omega t)$ |
| $\sim$ | = | state estimate |

## Introduction

ELECTRODYNAMIC tethers have the potential to play an important role in future spacecraft systems. They enable both power generation and orbital maneuvering without the expenditure of propellant by deploying an electrically conductive wire in the ionosphere and magnetic field of the Earth. As the tether cuts through the magnetic field, a potential difference is created, allowing a current to flow in the tether [1–3]. By proper control of the current, it is possible to alter all of the orbital elements of the spacecraft center of mass orbit [4,5] or to damp the tether librational modes [6–8].

The control of electrodynamic tethers is an important issue for the future use of tethers in space. A variety of feedback-control algorithms have been developed over the past several years, many of which assume a completely rigid tether [9–13]. Furthermore, full-state feedback has often been assumed in the work in the literature, due to the inherent instability of the system even under a constant current [14,15]. In reality, however, factors such as time delay, noisy measurements, and the effects of tether flexibility potentially make feedback control of electrodynamic tethers much more difficult.

The control of electrodynamic tethers on inclined orbits is important because of the inherent instability provided by the electric current [14]. Although the instability is a function of the magnitude of the current and can have a long time to double the amplitude, it must be controlled for long-term operations. There exists a unique libration cycle, however, for which the net energy input per orbit is zero. Such a libration cycle is a periodic solution to the equations of motion for the system [15]. The periodic solution is unstable for constant currents, with instability (magnitude of the moduli of monodromy matrix) growing with the electric current [14]. Periodic solutions have also been determined for tethers, including the lateral dynamics [16]. The instability in the lateral dynamics grows at a

Received 30 May 2009; revision received 29 October 2009; accepted for publication 29 October 2009. 

*Currently RMIT University, 1/4 Maylands Avenue, Balwyn North, VIC 3104, Australia; tethered.systems@gmail.com. Member AIAA.

faster rate than the librational instability. The effect of orbit eccentricity was shown by Peláez and Andres [17] to amplify the unstable nature of the dynamics. Hoyt [18] described schemes for stabilizing flexible electrodynamic tethers during deorbit by periodically measuring the motion of several points along the tether to estimate the oscillation energy and adjusting the control input accordingly. However, the requirement to measure specific points along the tether limits the practical application of this control scheme. It is likely to increase the costs of electrodynamic tethers, due to the need to embed additional sensors along the tether length. However, the results presented by Hoyt clearly demonstrate that knowledge of the tether shape at discrete points can be used to control the lateral vibrations of an electrodynamic tether.

Control of the unstable skip-rope motion during retrieval was shown by Williams et al. [8] to be effectively suppressed if a movable attachment point is used to damp the lateral oscillations of the electrodynamic tether. This control scheme used only information from the boundary conditions of the tether. Peláez and Lorenzini [10] addressed the issue of controlling the librations of an electrodynamic tether around the periodic solution. Their approach consisted of two linear feedback-control schemes. The first was simple proportional feedback for the in- and out-of-plane libration rates, and the second was a delayed-feedback version of the same controller. However, the implementations of these controllers were assumed to be independent, and it was suggested that control could be achieved using movement of the tether attachment point. For the case of a constant current, Williams [11] used an energy-rate feedback approach to stabilize the librational motion of the tether around the periodic solution by adjusting the amount of current flowing in the tether. Part 1 [19] of this paper showed that the energy-rate feedback approach also works for the case of a nonconstant current, in which the current is applied in a controlled manner for changing the orbital elements of the spacecraft. Part 1 [19] used a numerical algorithm based on the Legendre pseudospectral method [20] to determine the stability of periodic solutions of electrodynamic tethers under forced currents.

In all of the aforementioned work, exact state feedback has been assumed. In [13] a scheme based on model-predictive control using noisy measurements was shown to stabilize the librational motion of electrodynamic tethers to the periodic solution without any a priori knowledge of the periodic solution. The approach stabilizes the librations during orbital maneuvers and in the presence of a tilted magnetic field using estimated tether states. The effects of tether flexibility were not considered.

The goal of this paper is to develop a means for estimating the full tether state using a measured subset of the states. This paper investigates the use of a square-root unscented filter for estimating the dynamic motion of electrodynamic tethers. First, a filter is developed for an inelastic tether (classic rigid-dumbbell model), and an analytic feedback-control law is implemented using sampled data feedback with estimates generated via the filter. The effects of different measurement and process noises on the closed-loop response are examined. Next, a filter is developed using a lumped-mass tether model for predicting the tether shape. The filter is shown to be able to accurately predict the tether shape and libration dynamics using only measurements at the system end points. Reference periodic solutions for flexible tethers are generated by means of the Legendre pseudospectral method. The control law applied in Part 1 [19] is extended to deal with the lateral tether oscillation modes.

## Mathematical Models

### Dumbbell Model

In this work, a simplified tether model is used for studying the librational dynamics and for preliminary development of a libration estimator. In the next section, a discretized tether model that accounts for the tether lateral flexibility is introduced. The dumbbell model of the tether is adopted from Peláez and Lorenzini [10] and is illustrated in Fig. 1. The mother satellite is assumed to remain in a circular orbit, and the tether is modeled by a rigid rod undergoing forced librations

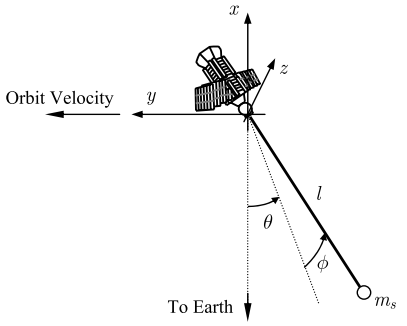


**Fig. 1 Three-dimensional tethered satellite dumbbell model.**

due to the electric current. The assumption of a circular orbit implies that the mother satellite is significantly larger in mass than the subsatellite and tether, which restricts the mass ratio of mother satellite to subsatellite to roughly larger than 100 and restricts tether lengths less than approximately 50 km. For more generality, the nondimensional parameter

$$\bar{\varepsilon} = \frac{f_e I \mu_m}{\mu(m_s + m_t/3)}$$

is used, where $f_e$ is a parameter governing the distribution of electric current along the tether, $I$ is the current, $\mu_m$ is the magnetic field strength, $\mu$ is the gravitational constant of the Earth, $m_s$ is the subsatellite mass, and $m_t$ is the tether mass. Essentially, the parameter $\bar{\varepsilon}$ governs the ratio of torque due to electrodynamics to the torque due to gravitational forces.

The nondimensional equations of motion are given by [15,19]

$$\theta'' = 2(\theta' + 1)\phi' \tan\phi - 3\sin\theta\cos\theta - \bar{\varepsilon}[\sin i \tan\phi(2\sin\nu\cos\theta - \cos\nu\sin\theta) + \cos i] \tag{1}$$

$$\phi'' = -\sin\phi\cos\phi[(\theta' + 1)^2 + 3\cos^2\theta] + \bar{\varepsilon}(2\sin\nu\sin\theta + \cos\nu\cos\theta)\sin i \tag{2}$$

The main assumption used in the derivation of the equations of motion is that the magnetic field is represented by a nontilted dipole. The tether tension is a function of the librational dynamics only and is given by

$$T = \left(m_s + \frac{m_t}{2}\right)\dot{\nu}^2 l[\phi'^2 + (\theta' + 1)^2\cos^2\phi + (3\cos^2\theta\cos^2\phi - 1)] \tag{3}$$

Note that for flexible tethers, the electrodynamic forces induce additional tension forces as a result of the curvature of the tether. Equation (3) does not take this effect into account. Equations (1) and (2) have periodic solutions that can be obtained by Poincare's method of the continuation of periodic orbits. Alternatively, periodic solutions can be generated via nonlinear programming, as described in Part 1 [19].

### Flexible-Tether Model

Peláez et al. [16] used a two-bar tether model to assess the effects of tether lateral flexibility on periodic solutions and their stability. The two-bar model essentially treats the tether as being composed of a double pendulum, with mass distributed along each pendulum. Later, Ruiz et al. [21] provided a modal analysis of a flexible electrodynamic tether using an assumed-modes approach. In this section, a model that fills the gap between these extremes is used. The effects of longitudinal vibrations are ignored, and the tether is divided into a series of point masses connected via inelastic links. Thus, the geometric shortening of the distance to the tether tip is accounted for due to the changes in geometry. The degree of approximation is

controlled by the number of discretized elements that are used. The modeling approach is useful for predicting the effects of control schemes applied to a flexible tether.

As shown in Fig. 2, the tether is modeled as consisting of a series of $n$ point masses connected via inelastic links. The $(x, y, z)$ coordinate system rotates at the orbit angular velocity and is assumed to be attached at the center of mass of the orbit. In general, this coordinate system would orbit in a plane defined by the classical orbital elements $(\Omega, i, \varpi)$. Although the orientation of the orbital plane does not affect the system dynamics in the presence of a Newtonian gravitational field, it does affect the electrodynamic forces, due to the nature of the Earth's magnetic field.

The nondimensional equations of motion can be written as [22]

$$\begin{aligned}\theta_j'' = {} & 2(\theta_j' + 1)\left[\phi_j' \tan\phi_j - \frac{\Lambda_j'}{\Lambda_j}\right] - 3\sin\theta_j\cos\theta_j \\ & - \frac{m_{j-1}}{m_j}\frac{u_{j-1}\sin\theta_j\cos\theta_{j-1}\cos\phi_{j-1}}{\Lambda_j\cos\phi_j} \\ & + \frac{m_{j-1}}{m_j}\frac{u_{j-1}\cos\theta_j\sin\theta_{j-1}\cos\phi_{j-1}}{\Lambda_j\cos\phi_j} \\ & + \frac{u_{j+1}\cos\theta_j\sin\theta_{j+1}\cos\phi_{j+1}}{\Lambda_j\cos\phi_j} - \frac{u_{j+1}\sin\theta_j\cos\theta_{j+1}\cos\phi_{j+1}}{\Lambda_j\cos\phi_j} \\ & + \frac{F_j^y\cos\theta_j}{m_j\omega^2 L\Lambda_j\cos\phi_j} - \frac{F_j^x\sin\theta_j}{m_j\omega^2 L\Lambda_j\cos\phi_j} + \frac{F_{j+1}^x\sin\theta_j}{m_{j+1}\omega^2 L\Lambda_j\cos\phi_j} \\ & - \frac{F_{j+1}^y\cos\theta_j}{m_{j+1}\omega^2 L\Lambda_j\cos\phi_j} \end{aligned} \tag{4}$$

$$\begin{aligned}\phi_j'' = {} & -2\frac{\Lambda_j'}{\Lambda_j}\phi_j' - [(\theta_j' + 1)^2 + 3\cos^2\theta_j]\sin\phi_j\cos\phi_j \\ & + \frac{m_{j-1}}{m_j}\frac{u_{j-1}}{\Lambda_j}(\cos\phi_j\sin\phi_{j-1} - \cos\theta_j\sin\phi_j\cos\theta_{j-1}\cos\phi_{j-1} \\ & - \sin\theta_j\sin\phi_j\sin\theta_{j-1}\cos\phi_{j-1}) \\ & + \frac{u_{j+1}}{\Lambda_j}(\cos\phi_j\sin\phi_{j+1} - \cos\theta_j\sin\phi_j\cos\theta_{j+1}\cos\phi_{j+1} \\ & - \sin\theta_j\sin\phi_j\sin\theta_{j+1}\cos\phi_{j+1}) \\ & + \frac{F_j^z\cos\phi_j}{m_j\omega^2 L\Lambda_j} - \frac{F_{j+1}^z\cos\phi_j}{m_{j+1}\omega^2 L\Lambda_j} + \frac{F_{j+1}^y\sin\theta_j\sin\phi_j}{m_{j+1}\omega^2 L\Lambda_j} \\ & - \frac{F_j^y\sin\theta_j\sin\phi_j}{m_j\omega^2 L\Lambda_j} - \frac{F_j^x\cos\theta_j\sin\phi_j}{m_j\omega^2 L\Lambda_j} + \frac{F_{j+1}^x\cos\theta_j\sin\phi_j}{m_{j+1}\omega^2 L\Lambda_j} \end{aligned} \tag{5}$$

$$\begin{aligned}\Lambda_j'' = {} & \Lambda_j[(\theta_j' + 1)^2\cos^2\phi_j + \phi_j'^2 - (1 - 3\cos^2\theta_j\cos^2\phi_j)] \\ & - u_j - \frac{m_j}{m_{j+1}}u_j + \frac{F_j^z\sin\phi_j}{m_j\omega^2 L} - \frac{F_{j+1}^z\sin\phi_j}{m_{j+1}\omega^2 L} + \frac{F_j^y\sin\theta_j\cos\phi_j}{m_j\omega^2 L} \\ & - \frac{F_{j+1}^y\sin\theta_j\cos\phi_j}{m_{j+1}\omega^2 L} + \frac{F_j^x\cos\theta_j\cos\phi_j}{m_j\omega^2 L} - \frac{F_{j+1}^x\cos\theta_j\cos\phi_j}{m_{j+1}\omega^2 L} \\ & + \frac{m_{j-1}}{m_j}u_{j-1}[\cos\theta_j\cos\phi_j\cos\theta_{j-1}\cos\phi_{j-1} + \sin\phi_j\sin\phi_{j-1} \\ & + \sin\theta_j\cos\phi_j\sin\theta_{j-1}\cos\phi_{j-1}] \\ & + u_{j+1}[\cos\theta_j\cos\phi_j\cos\theta_{j+1}\cos\phi_{j+1} + \sin\phi_j\sin\phi_{j+1} \\ & + \sin\theta_j\cos\phi_j\sin\theta_{j+1}\cos\phi_{j+1}] \end{aligned} \tag{6}$$

The boundary conditions to be applied to Eqs. (4–6) are

$$m_0 = 0, \qquad u_0 = 0, \qquad m_{n+1} = \infty, \qquad u_{n+1} = 0 \tag{7}$$

To simulate the case of a fixed-length tether, Eqs. (6) are set to zero for $j = 1, \ldots, n$, allowing the unknown nondimensional tensions $u_j$ $(j = 1, \ldots, n)$ to be determined. Note that these equations are linear in the unknown tensions, so the vector of $u_j$ can be obtained using Gaussian elimination. The tensions are a complex function of the external forces, due to electrodynamics, and the local segment angles and rates. The resulting tensions are substituted back into the librational dynamics to determine the evolution of the system dynamics.

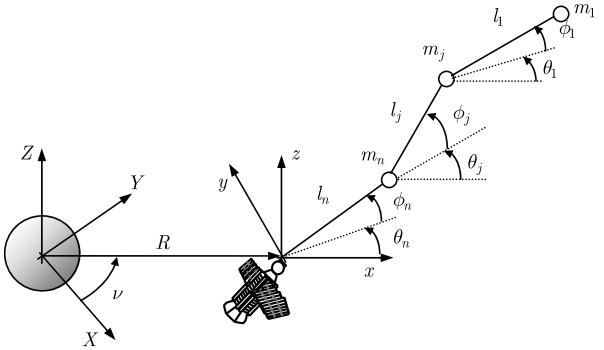


**Fig. 2 Discretized flexible electrodynamic tether model.**

#### Electrodynamic Forces

The electrodynamic forces acting along the tether are produced by the interaction of the conducting tether with the magnetic field:

$$\boldsymbol{F}^e := \begin{cases} \frac{1}{2}I\boldsymbol{p}_j \times \boldsymbol{B}, & j = 1 \\ \frac{1}{2}(I\boldsymbol{p}_{j-1} \times \boldsymbol{B} + I\boldsymbol{p}_j \times \boldsymbol{B}), & j = 2, \ldots, n \end{cases} \tag{8}$$

where

$$\boldsymbol{p}_j = l_j\cos\theta_j\cos\phi_j\boldsymbol{i} + l_j\sin\theta_j\cos\phi_j\boldsymbol{j} + l_j\sin\phi_j\boldsymbol{k} \tag{9}$$

is the local tether tangent vector, and

$$\begin{aligned}\boldsymbol{B} = {} & -2\frac{\mu_m}{R^3}\sin(\varpi + \nu)\sin i\boldsymbol{i} + \frac{\mu_m}{R^3}\cos(\varpi + \nu)\sin i\boldsymbol{j} \\ & + \frac{\mu_m}{R^3}\cos i\boldsymbol{k} \end{aligned} \tag{10}$$

is the local magnetic field vector, which is assumed to be constant along the tether length.

## Feedback Control for Libration and Flexible Mode Stabilization

In Part 1 [19], energy-rate feedback was demonstrated for tracking the periodic trajectory of an electrodynamic tether using current control with exact state feedback. This section extends the previous results to consider the practical case of a flexible tether.

The feedback controller for the libration dynamics is of the following form:

$$\bar{\varepsilon} = \bar{\varepsilon}_{\text{ref}}[1 - k_1(E - E_{\text{ref}})\text{sign}\bar{\varepsilon}_{\text{ref}}] \tag{11}$$

where $k_1$ is a feedback gain, and

$$\begin{aligned}E_{\text{ref}} = {} & \phi_{\text{ref}}'(2\sin\nu\sin\theta_{\text{ref}} + \cos\nu\cos\theta_{\text{ref}})\sin i \\ & - [\sin i\tan\phi_{\text{ref}}(2\sin\nu\cos\theta_{\text{ref}} - \cos\nu\sin\theta_{\text{ref}}) \\ & + \cos i]\theta_{\text{ref}}'\cos^2\phi_{\text{ref}} \end{aligned} \tag{12}$$

In [8], a libration control law was derived via Lyapunov's second method for suppressing the librations of a tether using electrodynamic forces. Part of the motivation for such a study was to determine whether or not electrodynamic forces are a viable means of manipulating the large-amplitude motions of the tether librations. The results clearly showed that although the control law works extremely well when implemented in the rigid tether model, it requires an additional control law to function properly for a flexible-tether system. In particular, as the energy is taken out of the tether

librations, some of it appears to be pumped into the tether skip-rope mode. If this is coupled with length variations of the tether, then large instabilities can be observed. To deal with this issue, a movable attachment point was used to damp the traveling waves in the tether. However, many future missions involving electrodynamic tethers may not be equipped with the ability to move the tether attachment points, and so it is of tremendous practical concern to be able to control the higher-order tether modes by some other means, preferably via the electric current itself.

An additional control law is proposed to remove energy from the tether lateral modes. The total control law for stabilizing the tether librations and lateral modes is given by

$$\bar{\varepsilon} = \bar{\varepsilon}_{\text{ref}} + \Delta\bar{\varepsilon}_{\text{librations}} + \Delta\bar{\varepsilon}_{\text{lateral}} \tag{13}$$

where

$$\Delta\bar{\varepsilon}_{\text{librations}} = -k_1\bar{\varepsilon}_{\text{ref}}(E - E_{\text{ref}})\text{sign}\bar{\varepsilon}_{\text{ref}} \tag{14}$$

$$\Delta\bar{\varepsilon}_{\text{lateral}} = k_2\bar{\varepsilon}_{\text{ref}}(\mathcal{E} - \mathcal{E}_{\text{ref}})\text{sign}\bar{\varepsilon}_{\text{ref}} \tag{15}$$

and $\mathcal{E}$ is defined similarly to Eq. (12), except that it uses a point of reference close to the main satellite. In the simulations in this paper, the point of reference is the first discretized mass. Essentially, this type of controller uses the same information as a movable attachment point, except that feedback is provided via modulations in the electric current. To make the controller practical, it must be coupled with a state estimator. This is the subject of the next section.

## Estimation of Tether States

The tether system is composed of rigid-body librations and flexible modes that require active control to avoid instabilities. The most problematic mode for an electrodynamic tether is the skip-rope mode, in which the tether bows and rotates around an axis connecting the main satellite and subsatellite. To control the skip-rope mode, it is necessary to be able to estimate the tether shape. One approach to estimating the tether shape is to embed sensors at discrete positions along the tether length. Provided that enough sensors are used, the measurements can be used to directly estimate the oscillation energy in the tether. This approach was used by Hoyt [18]. A more practical approach might be to use sensors only on at the boundary points of the tether, i.e., on the main satellite and the subsatellite. The goal of this section is to consider a mathematical framework in which a reduced discrete tether state can be estimated by means of two complementary sensors: Global Positioning System (GPS) position measurements of the subsatellite position and a three-axis tension sensor on the main satellite. This is a classical nonlinear state-estimation problem for which established algorithms exist. This section will outline the estimation problem and then describe the method used to solve it in a recursive fashion.

### Libration State Estimation of a Rigid Tether

In the following, it is assumed that the orbit of the base satellite is known. The goal of the state estimation, therefore, is to estimate the relative motion of the tether and subsatellite. The approach used here is to use a three-axis tension sensor on the main spacecraft, combined with knowledge of the deployed tether length. Knowledge of the tether tension vector provides information about the tether direction as well as dynamic information about the subsatellite motion. A tension sensor has other important roles in tether control, such as providing important feedback data during deployment [23]. The tension sensor would provide the components of the tension vector in the spacecraft body frame (i.e., body frame of the mother satellite). Since the tether dynamic model expresses the tension forces in the orbital frame, it is straightforward to relate the satellite body frame to the orbital frame:

$$\boldsymbol{T}_{\text{orbital}} = [C_B^O]\boldsymbol{T}_{\text{body}} \tag{16}$$

where $C_B^O$ is the transformation matrix relating the spacecraft body frame $B$ to the orbital frame $O$. For simplicity, the body frame and orbital frame are assumed to coincide in this paper, i.e., $C_B^O = \boldsymbol{I}_{3\times3}$. This means that the attitude of the mother spacecraft is assumed to be controlled such that it always maintains alignment with the local vertical and is unperturbed by the effects of the tether. However, the tether is still free to librate under its own dynamics. It is relatively straightforward to consider other relationships, but this would require an attitude filter for the main spacecraft and coupling between the satellite attitude dynamics and the tether dynamics to be modeled. In any case, the onboard inertial system on the mother spacecraft is assumed to provide the means of transforming the tension vector in the body frame to the orbital frame.

The measurement model can be written as

$$\begin{aligned}
y_1 = T_x &= \left(m_s + \frac{m_t}{2}\right)\dot{\nu}^2 l[\phi'^2 + (\theta' + 1)^2\cos^2\phi \\
&\quad + (3\cos^2\theta\cos^2\phi - 1)]\cos\theta\cos\phi + b_{T_x}^r + w_{T_x}^r \\
y_2 = T_y &= \left(m_s + \frac{m_t}{2}\right)\dot{\nu}^2 l[\phi'^2 + (\theta' + 1)^2\cos^2\phi \\
&\quad + (3\cos^2\theta\cos^2\phi - 1)]\sin\theta\cos\phi + b_{T_y}^r + w_{T_y}^r \\
y_3 = T_z &= \left(m_s + \frac{m_t}{2}\right)\dot{\nu}^2 l[\phi'^2 + (\theta' + 1)^2\cos^2\phi \\
&\quad + (3\cos^2\theta\cos^2\phi - 1)]\sin\phi + b_{T_z}^r + w_{T_z}^r
\end{aligned} \tag{17}$$

where $w_{T_x}^r$, $w_{T_y}^r$, and $w_{T_z}^r$ are components of the measurement noise vector, and $b_{T_x}^r$, $b_{T_y}^r$, and $b_{T_z}^r$ are components of tension bias. This measurement noise vector takes into account sensor noise as well as the noise induced by the measurement model itself, i.e., the dumbbell model assumption. The measurement noise is assumed to follow a Gaussian white noise process with zero mean and covariance $\boldsymbol{R}^r \in \mathbb{R}^{3\times3}$. Note that in this model, the tether length is fixed and is assumed to be known. The tether length can be measured quite accurately from the number of turns of the tether on the spool. Alternatively, a fixed amount of tether could be deployed, for which the length would be known a priori. In any case, any inaccuracies in the tether length are subsumed into the measurement noise and bias estimates. It should be noted that significant steady-state errors in the tether length, subsatellite mass, or tether mass, would result in nonconstant biases even in the idealized tether model. Thus, the biases would need to be modeled using a random-walk process driven by white noise. In the remainder of this paper, the biases are assumed to be zero.

The goal of the estimation process is to use measurements of the tension vector to estimate the full tether state $\boldsymbol{x} = \{\theta, \theta', \phi, \phi'\}$ in a recursive fashion. The state estimates are used for applying feedback control to the system.

### Flexible-Tether State Estimation

Libration state estimation is only part of the requirements for a real electrodynamic tether system. It will be necessary to provide some means of estimating the tether lateral dynamics, particularly if the skip-rope mode is to be effectively suppressed. The measurement of the tension vector provides important information about the tether state, but it is not enough to provide accurate full tether state estimates. An additional sensor is required. Here, the position of the subsatellite is also assumed to be measured, which can be obtained through the use of GPS on the subsatellite for low orbital altitudes.

#### *Measurement Model*

The measurement model can be written using the states of the discrete tether model as

$$
\begin{aligned}
y_1 &= T_x^f = u_n m_n \omega^2 L \cos\theta_n \cos\phi_n + b_{T_x}^f + w_{T_x}^f \\
y_2 &= T_y^f = u_n m_n \omega^2 L \sin\theta_n \cos\phi_n + b_{T_y}^f + w_{T_y}^f \\
y_3 &= T_z^f = u_n m_n \omega^2 L \sin\phi_n + b_{T_z}^f + w_{T_z}^f \\
y_4 &= x_1 = \sum_{j=1}^{n} l_j \cos\theta_j \cos\phi_j + w_{x_1}^f \\
y_5 &= y_1 = \sum_{j=1}^{n} l_j \sin\theta_j \cos\phi_j + w_{y_1}^f \\
y_6 &= z_1 = \sum_{j=1}^{n} l_j \sin\phi_j + w_{z_1}^f
\end{aligned} \tag{18}
$$

where the superscript $f$ refers to the fact that we are dealing with flexible-tether state estimates. The biases on the tether tension are used to account for long-term instability of the tension. However, they are not included in the numerical analyses conducted in this paper. The errors in position are assumed to be Gaussian with zero mean and covariance $\boldsymbol{R}^f \in \mathbb{R}^{3\times3}$. Note that processed GPS data are assumed to be used and converted into a relative measurement in the orbital frame. In reality, position measurements obtained via GPS depend on the number of satellites in view by the antenna, their relative positions, receiver clock errors, and so on, which usually result in position errors to be non-Gaussian. These types of errors can be modeled using more sophisticated approaches. However, Gaussian errors are typically assumed in filter development, which usually requires inflated measurement covariances to be used because the assumption of Gaussian errors is violated in practice.

One of the advantages of the discrete model formulated in this paper is that it uses a minimum of generalized coordinates. Furthermore, if the Cartesian coordinates of the subsatellite are measured, this improves the observability of the full-state vector, due to the fact that the end mass position is a function of all the generalized coordinates. Unlike the case of the dumbbell model, the tension vector at the main spacecraft, $u_n$, cannot be written as an explicit function of the tether states for the discretized model used here. This has important implications for the filter development and algorithm selection.

*State Model*

The state equations used by the filter must be expressed in the form of a discrete-time update

$$\boldsymbol{x}_k = f(\boldsymbol{x}_{k-1}, \boldsymbol{u}_{k-1}, t_{k-1}) \tag{19}$$

The continuous equations of motion for the tether, defined in Eqs. (4–6), can be converted into discrete-time form using a suitable numerical integration technique. An Euler discretization offers the simplest approach with low numerical cost per time step. However, small time steps are required to adequately capture the high-frequency modes of the tether oscillations and to prevent the projections from diverging. This requires the use of a very small time step for an Euler discretization, which increases the overall amount of computation needed by the projection phase. Instead, a fourth-order Runge–Kutta algorithm is used to propagate the continuous time equations using a fixed time step, which allows larger time steps to be used.

**Implementation of Combined State Estimation and Feedback Control**

In general, the discretized time used by the state estimator may not coincide with the time that a measurement is taken. In addition, the sampling time of the state projection is typically smaller than the time step between measurement updates. Furthermore, due to delays in the transmission of data, the time at which measurements are received by the state estimator are not the same as the time at which the measurement was taken. Hence, it is important to address the problem of disparate sampling times for implementation of a practical estimator.

Figure 3 illustrates the block diagram of the implementation of the filter and control algorithm. The process begins with the state estimate from the previous step $(k-1)$, which is used in the process model to project forward to the current time step $(k)$. A corresponding measurement at the same time is used to update the state estimate. It should be noted that the discrete step from $k-1$ to $k$ may involve multiple integration steps, depending on the sensitivity of the system. If the filter runs at the same rate as the controller, then the current state estimate is used to update the feedback controller in a discrete manner. In this paper, it is assumed that the controller is updated at a faster rate than the state estimates. This can be handled in a few ways:

1) A zero- or first-order hold can be used on the state estimates.

2) A zero- or first-order hold can be used on the control signal computed from the latest available state estimate.

3) The model can be used to predict the state forward from the latest available state estimate with the feedback controller applied to generate a control signal to be applied to the real system.

The latter approach is used here and is shown in Fig. 3. This is a form of nonoptimal model-predictive control because feedback in the model is used to generate the actual control signal.

Because the system is nonlinear, it is necessary to employ a nonlinear filter such as the extended Kalman filter (EKF). However, the EKF can suffer from divergence and inconsistency problems, due to the linearization of the statistical models around the current best estimate. To better handle the transformation of Gaussian distributions through arbitrary nonlinear functions, the unscented filter was developed in [24]. The implementation of the filter in square-root form [25] helps to mitigate the effect of round-off errors as well as ensures that the covariance matrix remains positive semidefinite. The advantages of the unscented filter become apparent when it is understood that the EKF could not be applied without using numerical linearization to obtain the required system Jacobians. Numerical linearization is necessary because the state model is not written in closed analytical form. The unscented filter, on the other hand, does not require any explicit linearization because it uses a minimum number of sigma points that are designed to capture the mean and covariance of probability distributions propagated through arbitrary nonlinear functions. Thus, the unscented filter can be implemented without the need to derive analytic Jacobians, which makes it particularly attractive for estimating the states of an electrodynamic tether.

**Unscented Filtering**

The unscented filtering development presented here is based on the work presented in [25]. The system model is assumed to be of the form

$$\boldsymbol{x}_{k+1}^s = \boldsymbol{f}(\boldsymbol{x}_k^s, \boldsymbol{v}_k, \boldsymbol{u}_k, t_k) \tag{20}$$

$$\boldsymbol{y}_k = \boldsymbol{h}(\boldsymbol{x}_k^s, \boldsymbol{w}_k, \boldsymbol{u}_k, t_k) \tag{21}$$

where $\boldsymbol{x}_k^s$ is the state vector, $\boldsymbol{v}_k$ is a zero-mean Gaussian process noise with covariance $\boldsymbol{Q}_k$, $\boldsymbol{u}_k$ is the control input, $\boldsymbol{w}_k$ is a zero-mean Gaussian measurement noise with covariance $\boldsymbol{R}_k$, and $\boldsymbol{y}_k$ are the measured outputs. The functions $\boldsymbol{f}(\,)$ and $\boldsymbol{h}(\,)$ are general nonlinear

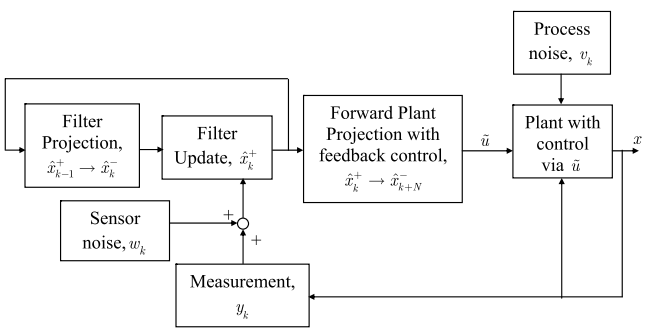


**Fig. 3 Block diagram of combined filter and feedback controller.**

functions, but are assumed to have known structures. The presence of process noise accounts for the fact that control inputs may not be known exactly, as well as allowing for errors in modeling.

In the following, we implicitly augment the state vector with the process and measurement noise as follows:

$$\boldsymbol{x}_k = \begin{bmatrix} \boldsymbol{x}_k^s \\ \boldsymbol{w}_k \\ \boldsymbol{v}_k \end{bmatrix} \tag{22}$$

The first step in the filter is to compute the set of sigma points as follows:

$$\mathcal{X}_{k-1} = [\hat{\boldsymbol{x}}_{k-1}, \hat{\boldsymbol{x}}_{k-1} + \gamma \boldsymbol{S}_k, \hat{\boldsymbol{x}}_{k-1} - \gamma \boldsymbol{S}_k] \tag{23}$$

where $\hat{\boldsymbol{x}}$ is the mean estimate of the state vector, $\boldsymbol{S}_k$ is the Cholesky form of the covariance matrix, and the parameter $\gamma$ is defined by

$$\gamma = \sqrt{L + \lambda} \tag{24}$$

where $\lambda = \alpha^2(L + \kappa) - L$ is a scaling parameter, with the values of $\alpha$ and $\kappa$ selected appropriately, and the length $L$ denotes the length of the augmented state vector. The sigma points are then propagated through the nonlinear dynamics as follows:

$$\mathcal{X}^*_{k|k-1} = \boldsymbol{f}(\mathcal{X}_{k-1}, \boldsymbol{u}_k, t_k) \tag{25}$$

The predicted mean for the state estimate is calculated from

$$\hat{\boldsymbol{x}}_k^- = \sum_{i=0}^{2L} W_i^{\text{mean}} \mathcal{X}^*_{i,k|k-1} \tag{26}$$

where

$$W_i^{\text{mean}} = \begin{cases} \frac{\lambda}{L+\lambda}, & i = 0 \\ \frac{1}{2(L+\lambda)}, & i = 1, \ldots, 2L \end{cases} \tag{27}$$

The Cholesky form of the covariance is predicted using

$$\boldsymbol{S}_k^- = \text{qr}[\sqrt{W_1^{\text{cov}}}(\mathcal{X}^*_{1:2L,k|k-1} - \hat{\boldsymbol{x}}_k^-), \sqrt{\boldsymbol{Q}_k}] \tag{28}$$

$$\boldsymbol{S}_k^- = \text{Cholupdate}\{\boldsymbol{S}_k^-, \mathcal{X}^*_{0,k} - \hat{\boldsymbol{x}}_k^-, W_0^{\text{cov}}\} \tag{29}$$

where

$$W_i^{\text{cov}} = \begin{cases} \frac{\lambda}{L+\lambda} + (1 - \alpha^2 + \beta), & i = 0 \\ \frac{1}{2(L+\lambda)} & i = 1, \ldots, 2L \end{cases} \tag{30}$$

qr{} represents the QR decomposition of the matrix, and Cholupdate{} represents the Cholesky factor update. Next, the propagated sigma points are augmented by

$$\mathcal{X}_{k|k-1} = [\mathcal{X}^*_{k|k-1}, \mathcal{X}^*_{k|k-1} + \gamma\sqrt{\boldsymbol{Q}_k}, \mathcal{X}^*_{k|k-1} - \gamma\sqrt{\boldsymbol{Q}_k}] \tag{31}$$

The augmented sigma points are propagated through the measurement equations

$$\mathcal{Y}_{k|k-1} = \boldsymbol{h}(\mathcal{X}_{k|k-1}, \boldsymbol{u}_k, t_k) \tag{32}$$

The mean predicted observation is obtained by

$$\hat{\boldsymbol{y}}_k^- = \sum_{i=0}^{2L} W_i^{\text{mean}} \mathcal{Y}_{i,k|k-1} \tag{33}$$

The output Cholesky covariance is calculated using

$$\boldsymbol{S}_{\tilde{\boldsymbol{y}}_k} = \text{qr}[\sqrt{W_1^{\text{cov}}}(\mathcal{Y}_{1:2L,k} - \hat{\boldsymbol{y}}_k^-), \sqrt{\boldsymbol{R}_k}] \tag{34}$$

$$\boldsymbol{S}_{\tilde{\boldsymbol{y}}_k} = \text{Cholupdate}\{\boldsymbol{S}_{\tilde{\boldsymbol{y}}_k}, \mathcal{Y}_{0,k} - \hat{\boldsymbol{y}}_k^-, W_0^{\text{cov}}\} \tag{35}$$

The cross-correlation matrix is determined from

$$\boldsymbol{P}_{\boldsymbol{x}_k\boldsymbol{y}_k} = \sum_{i=0}^{2L} W_i^{\text{cov}}(\mathcal{X}_{i,k|k-1} - \hat{\boldsymbol{x}}_k^-)(\mathcal{Y}_{i,k|k-1} - \hat{\boldsymbol{y}}_k^-)^T \tag{36}$$

The gain for the Kalman update equations is computed from

$$\mathcal{K}_k = (\boldsymbol{P}_{\boldsymbol{x}_k\boldsymbol{y}_k} / \boldsymbol{S}_{\tilde{\boldsymbol{y}}_k}^T) / \boldsymbol{S}_{\tilde{\boldsymbol{y}}_k} \tag{37}$$

The state estimate is updated with a measurement using

$$\hat{\boldsymbol{x}}_k = \hat{\boldsymbol{x}}_k^- + \mathcal{K}_k(\boldsymbol{y}_k - \hat{\boldsymbol{y}}_k^-) \tag{38}$$

and the covariance is updated using

$$\boldsymbol{S}_k = \text{Cholupdate}\{\boldsymbol{S}_k^-, \mathcal{K}_k \boldsymbol{S}_{\tilde{\boldsymbol{y}}_k}, -1\} \tag{39}$$

The unscented state-estimation algorithm is implemented in MATLAB together with the tether models and feedback controllers. In practice, the filter process and measurement covariances need to be tuned carefully to obtain satisfactory results. The effectiveness of the proposed approaches is assessed in the numerical results that follow.

## Numerical Results

This section presents the results of numerical simulations conducted using models implemented in MATLAB. First, estimation of the tether librations using tension measurements is investigated. The results are used to close the loop using energy-rate feedback. Next, the estimation of the states of a flexible electrodynamic tether is undertaken. Finally, results of the closed-loop simulations using estimated state data are presented. Numerical propagation of closed-loop trajectories were performed using a fourth-order Runge–Kutta algorithm with adaptive step control with relative and absolute tolerances of $10^{-12}$. Periodic solutions were generated by means of the Legendre pseudospectral method with 150 nodes, as outlined in Part 1 [19]. The parameters used in the unscented filter were selected as $\alpha = 0.5$, $\beta = 2$, and $\kappa = 3 - L$.

### Dumbbell Model Estimation

*Effect of Measurement Noise on State Estimates*

To examine the filter performance for an electrodynamic tether system using measurements of the tension vector, a series of simulations were undertaken using the periodic solution for an electrodynamic tether in a 45-deg-inclination orbit with $\varepsilon = 1.5$, i.e., a constant current. The true solution is the periodic solution repeated an arbitrary number of times. No feedback control is used to control the tether motion. The effect of measurement noise on the filtered estimates is important for assessing how well both the filter and the use of tension measurements can be used for estimating the tethered satellite motion.

Measurement noise covariances of the form $R = \text{diag}[\sigma_x^2, \sigma_y^2, \sigma_z^2]$ were simulated with $\sigma_x = \sigma_y = \sigma_z = \sigma$, and $\sigma = [0.25, \ldots, 5]$ N at steps of 0.25 N. The same initial covariance

$$\boldsymbol{P}_0 = \text{diag}\left[\left(\frac{\pi}{6}\right)^2, \left(\frac{\pi}{6}\right)^2, \left(\frac{\pi}{6}\right)^2, \left(\frac{\pi}{6}\right)^2\right]$$

and state error were used in all cases (normally distributed with standard deviation $\pi/6$ on all states). Furthermore, the same random seed was used to ensure that the only variable affecting the results is the amplitude of the measurement noise.

It has been found that the use of spherical angles can cause problems with initial convergence of the unscented filter, and the resulting solution can jump to another region of the state space where the solution is a multiple of $\pi$ or $2\pi$. It should be noted that in the dumbbell model, the $\theta = 0$ and $\theta = \pi$ solutions produce identical in-plane solutions and therefore tension measurements. However, the presence of the electrodynamic forces generates a unique solution unless $\phi = \pi$ as well. It can be easily verified that $\theta = \pi$ and $\phi = \pi$ is the same Cartesian position as $\theta = \phi = 0$. All solutions can be delineated by converting the state estimates into the set of unique Cartesian coordinates defined as follows:

$$x = l\cos\theta\cos\phi, \qquad y = l\sin\theta\cos\phi, \qquad z = l\sin\phi \tag{40}$$

The nondimensional time derivative of Eq. (40) is calculated assuming a fixed-length tether:

$$\begin{aligned} x' &= -l\theta'\sin\theta\cos\phi - l\phi'\cos\theta\sin\phi \\ y' &= l\theta'\cos\theta\cos\phi - l\phi'\sin\theta\sin\phi \qquad z' = l\phi'\cos\phi \end{aligned} \tag{41}$$

The reference periodic solution used for this analysis is shown in Fig. 4. As an example, consider the solution for the lowest-noise case in which $\sigma = 0.25$ N. The subsatellite mass is assumed to be 200 kg, the tether length is 10 km, and the tether mass is 10 kg. An example of the variation of the tension measurements is shown in Fig. 5, which shows the variation of the mean tension with the tether dynamic state, as well as the effect of the low-amplitude noise on the tension. This is repeated for several orbits of the tether system (although the noise in the tension will vary for each orbit).

The filter is implemented with a process noise of $Q = [10^{-6}, 10^{-2}, 10^{-6}, 10^{-2}]$ with the state vector defined as $\boldsymbol{x}^s = [\theta, \theta', \phi, \phi']$. Throughout the results, all filters are implemented with a sampling time of 1 s, but measurements are only fused with a sample time of 10 s. Figure 6a shows the errors in the nondimensional Cartesian coordinates of the tether tip as a function of time, parameterized with respect to the measurement noise, and Fig. 6b shows the standard deviation of the state errors averaged over five orbits. These results show that the largest errors occur for the lowest-noise case, $\sigma = 0.25$ N. This is due to the fact that the errors are measured from filter initiation. In the low-noise case, the states wrap to a different angle representation, which causes the filter to converge more slowly and with larger errors initially, as highlighted in Fig. 6a. These initial errors are not reflected in the filter covariance. Aside from this exception, the state errors generally increase slowly with the standard deviation on the measurement noise. The most accurate Cartesian state is the $x$ coordinate, and the least accurate is the out-of-plane velocity. The results show that the filter is able to converge with large errors in the estimates.

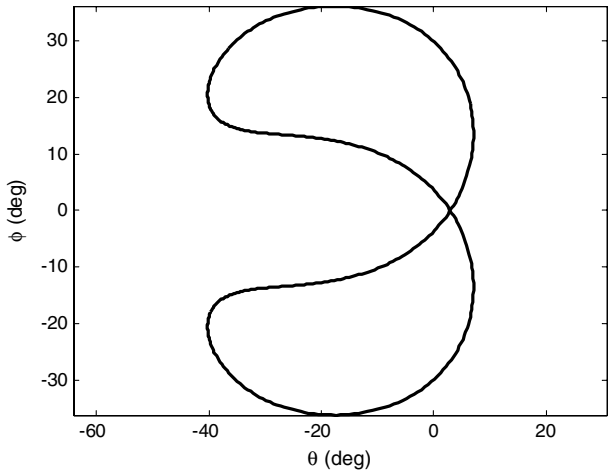


**Fig. 4 Reference periodic solution of dumbbell model for 45-deg-inclination circular orbit and $\varepsilon = 1.5$.**

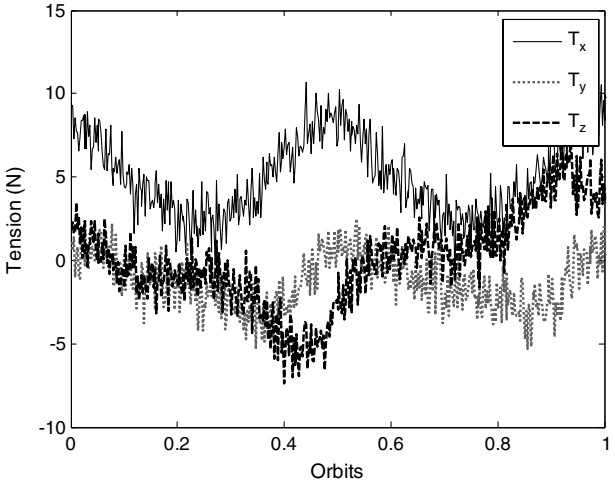


**Fig. 5 Tension measurements for 10-km-long tether with 200 kg subsatellite and $\sigma = 1$ N.**

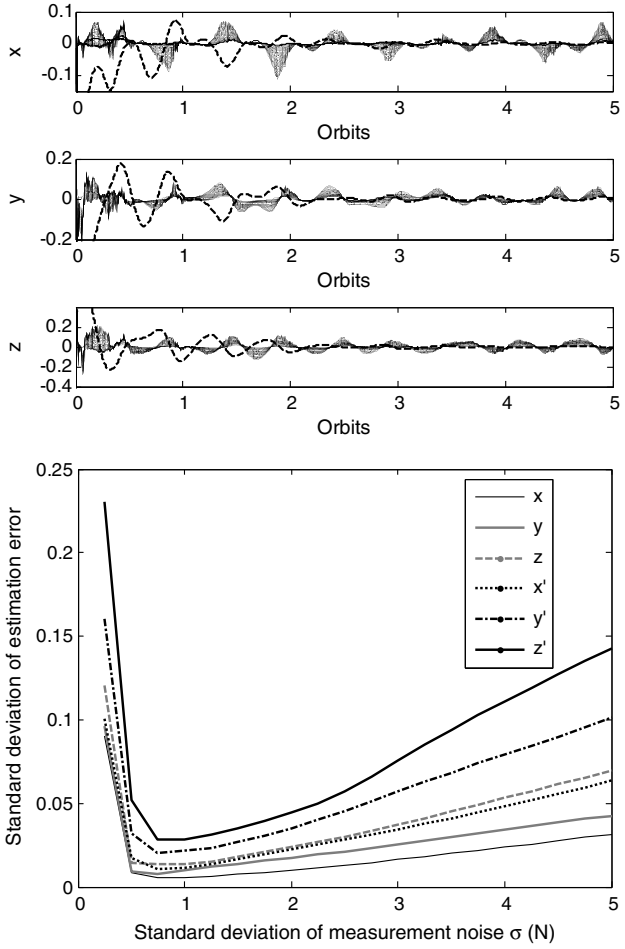


**Fig. 6 Plots of a) error in nondimensional Cartesian coordinates of tether tip using tension measurements, shown as a function of time for different measurement noise values (dashed lines are $\sigma = 0.25$ N) and b) standard deviation of estimation error versus standard deviation of measurement noise.**

*Effect of Imperfect State Feedback on Closed-Loop Control*

The results of the previous section illustrate that tension measurements can be used to obtain reasonably accurate libration estimates for the electrodynamic tether system. An important issue is whether the feedback controller proposed in Eq. (11) is robust enough to enable stabilization of the electrodynamic tether without perfect state feedback and the inevitable lag in the estimation of velocity states. This will be assessed by considering control of an electrodynamic tether with a time-varying reference current. The reference current is given by $\varepsilon = 1.2(1 + 0.5\sin 2\nu)$, and the inclination of the orbit is selected as 25 deg. A random disturbance is applied to the initial tether state and filter state with standard deviation of 0.1 rad. As in the previous section, various measurement noise values were used to assess its influence on the feedback controller. The feedback-control gain was selected as $k_1 = 3$.

Numerical results for the state estimation during the application of the feedback controller are shown in Fig. 7 for the case in which $\sigma = 4$ N. These results show that the state-estimation errors are

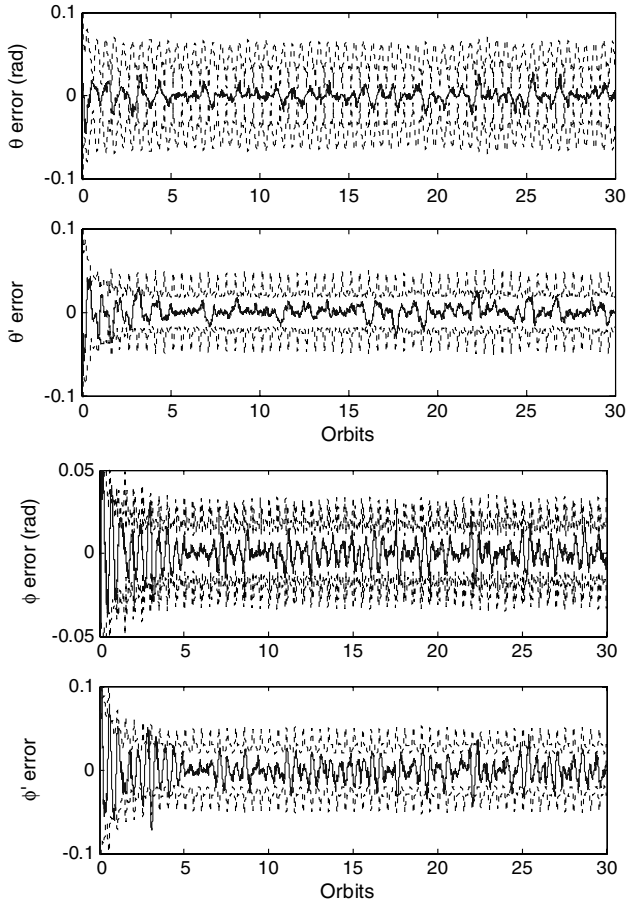


**Fig. 7 State estimation errors during feedback control with $\sigma = 4$ N (solid lines are state errors and dashed lines are 99% error bounds).**

consistent with predicted error covariances produced by the filter. The mean absolute error in the in-plane libration angle is 0.32 deg, and the mean absolute error in the out-of-plane libration angle is 0.34 deg. This shows very high accuracy for the state estimates, considering the large amount of noise on the tension measurements. Figure 8 shows the resulting closed-loop trajectories of the subsatellite for various measurement noises. It is clear from this plot that the smaller the measurement noise, the better the resulting closed-loop performance. Aside from this intuitive result, the plot shows that all closed-loop trajectories remain stable over the 30-orbit simulation. Hence, the energy-rate feedback controller remains stable in the presence of imperfect state feedback.

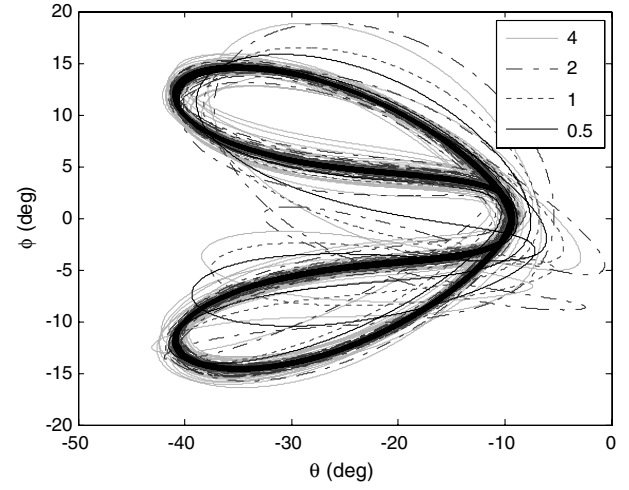


**Fig. 8 Closed-loop true state trajectories (noise values in newtons).**

*Periodic Trajectory and Feedback Control with Flexible Tether*

To demonstrate the applicability of the methods proposed in this paper, the case of a flexible electrodynamic tether is dealt with next. The physical parameters of the electrodynamic tether for these computations were selected as follows: the tether length is taken to be 10 km, the subsatellite mass is 50 kg, the tether mass density is 1 kg/km, the orbit inclination is 45 deg, and the orbit radius is 6870 km. For the computation of the periodic trajectory, the tether is discretized into eight masses, and the applied current is $I = 1 + 0.25 \sin 2\nu$ A. Figure 9 shows the periodic solution for the flexible electrodynamic tether in the orbital frame. The trajectory of the tether tip is very similar to the librational solution obtained for the rigid tether, but the tether does not remain straight between the end points. The periodic solution shown in Fig. 9 is unstable. The main source of instability is due to the tether lateral modes, which destabilize the system much more quickly than librational instabilities. To demonstrate, consider the case in which the tether librations are disturbed and a pure libration feedback controller is applied to the system. Simulation results are shown in Fig. 10 for a feedback gain of $k_1 = 2$. The lateral tether dynamics can be seen to approach extremely large amplitudes in a very short time (less than three orbits). Figure 10 illustrates that feedback of the subsatellite state is insufficient to stabilize the tether. By superimposing an additional control current on the reference current, closed-loop stability can be achieved. The results of the simulation with feedback gains of $k_1 = 2$ and $k_2 = 0.45$ are shown in Fig. 11. The results clearly show that both the librations and flexible modes are stabilized around the periodic solution. The motion of the subsatellite is shown in Fig. 12, and the motion of the tether midpoint is shown in Fig. 13.

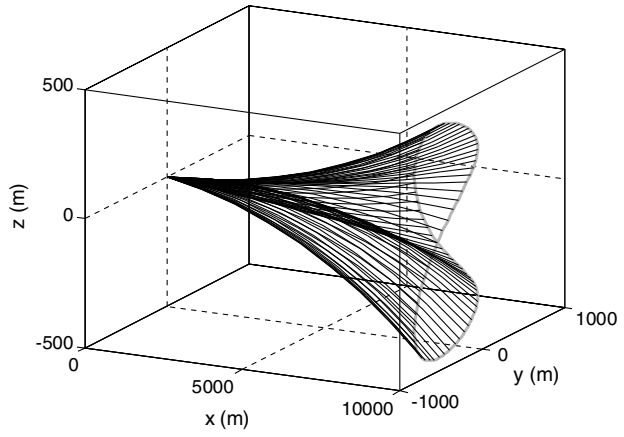


**Fig. 9 Reference periodic solution for a flexible electrodynamic tether under forced-current variations.**

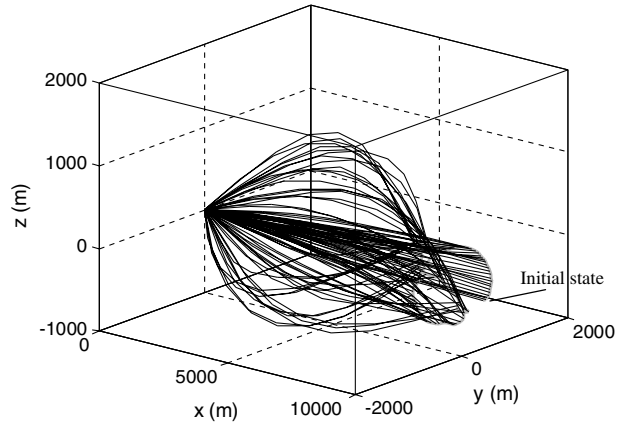


**Fig. 10 Example of libration-only feedback of flexible electrodynamic tether, $k_1 = 2$.**

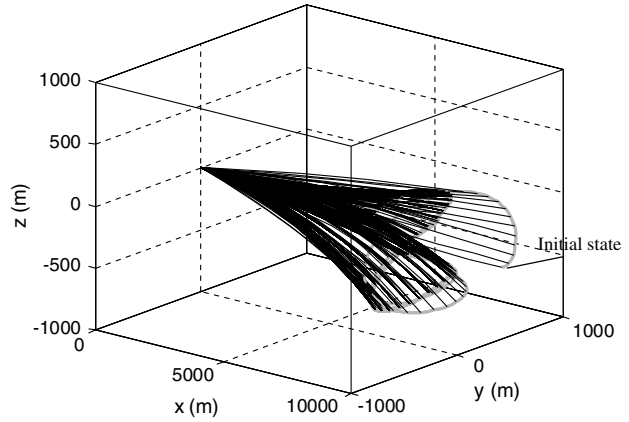


**Fig. 11 Example of stabilized libration and lateral tether dynamics using exact feedback, $k_1 = 2$ and $k_2 = 0.45$.**

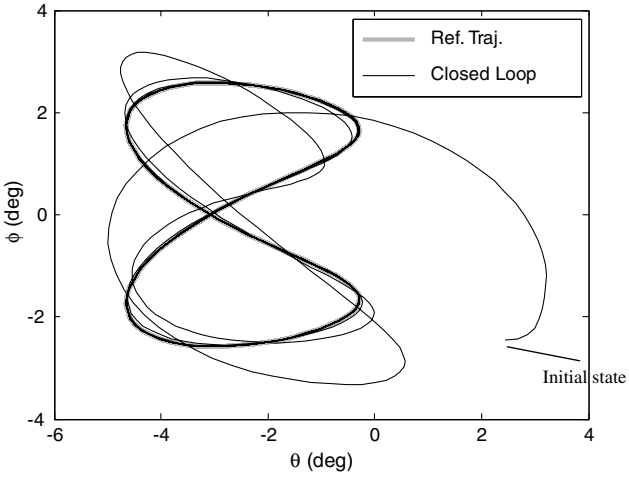


**Fig. 12 Librational component of closed-loop flexible electrodynamic tether.**

The librational response of the tether is generally similar to the response of a controlled rigid tether, whereas the motion of the midpoint has considerably higher frequency content due to the lateral tether modes. Figure 13 confirms that the tether enters into the desired periodic solution, including motion of the tether midpoint. Figure 14 shows the current applied to perform the feedback, illustrating reasonably rapid convergence to the reference current.

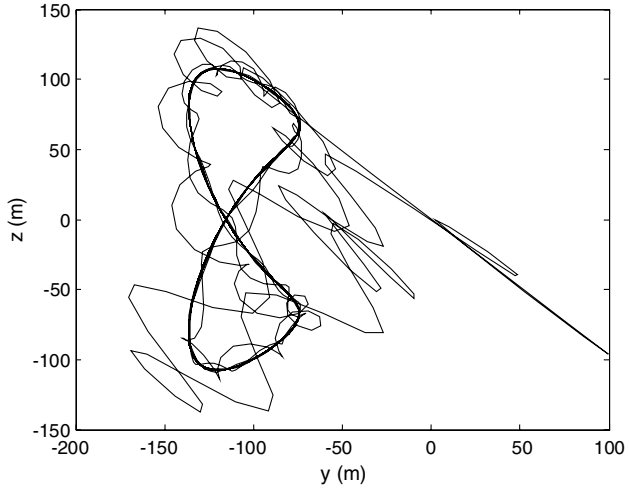


**Fig. 13 Motion of tether midpoint during controlled motion of flexible electrodynamic tether.**

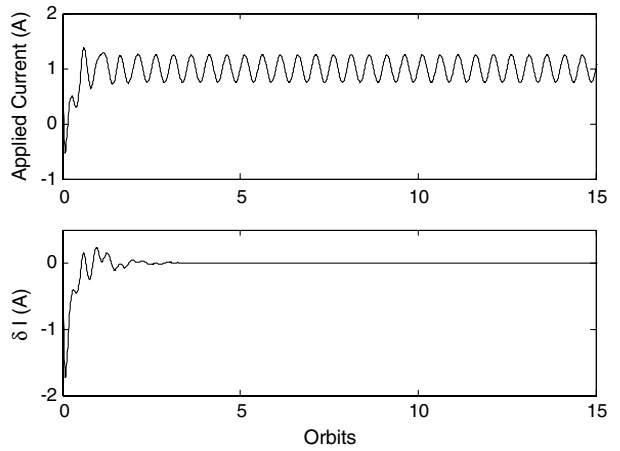


**Fig. 14 Plots of a) applied current during control of flexible electrodynamic tether and b) feedback current.**

To further illustrate the applicability of the feedback controller, the case is considered in which there is an initial disturbance to the tether shape only. That is, the position and velocity of the tether tip matches the desired periodic solution, but the amplitude of the lateral motion is altered from the periodic solution. Figure 15 shows simulation results for the libration component of the closed-loop simulation, illustrating that the libration dynamics are virtually unaltered by the disturbance. Figure 16 shows that the initial disturbance to the lateral

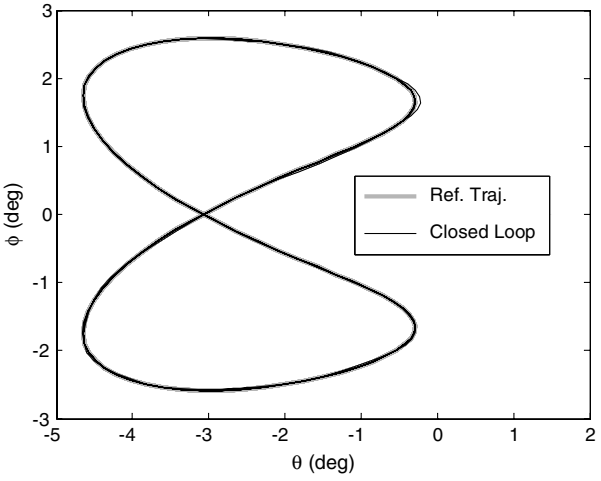


**Fig. 15 Libration dynamics for feedback control of electrodynamic tether with initial disturbance to tether shape.**

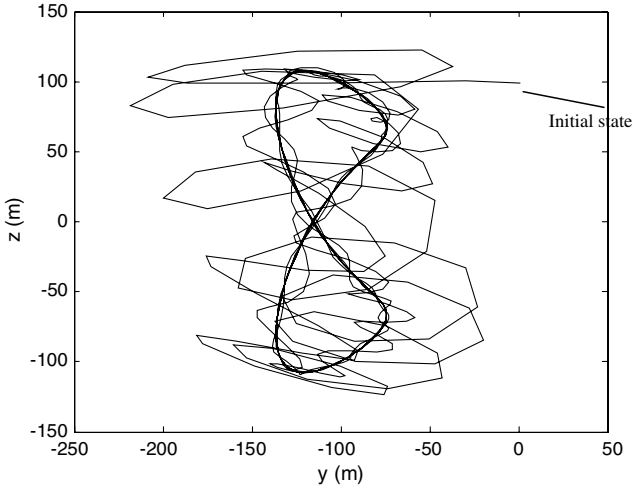


**Fig. 16 Motion of tether midpoint for feedback control of electrodynamic tether with initial disturbance to tether shape.**

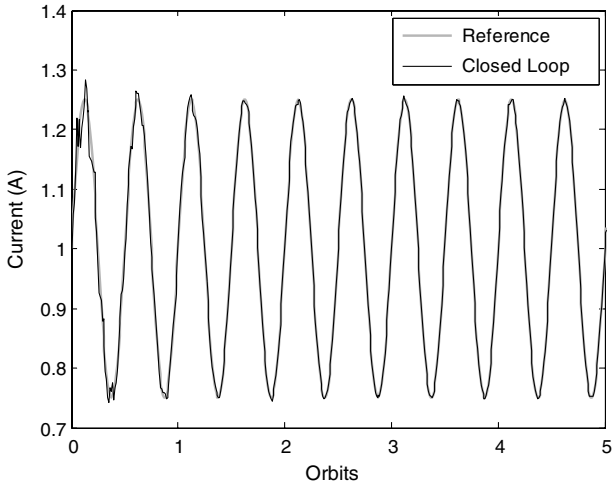


**Fig. 17 Applied current for feedback control of electrodynamic tether with initial disturbance to tether shape.**

dynamics is approximately 100 m for the position of the tether midpoint. The resulting closed-loop trajectory shows that the lateral vibrations are stabilized quite well by the feedback-control law. Finally, Fig. 17 shows the applied current necessary to stabilize the tether lateral dynamics. It can be seen that the control corrections are only relatively minor, demonstrating the good closed-loop performance of the controller.

**Electrodynamic Tether Shape Estimation and Control**

In this section, the unscented filter is applied to the full estimation of the states of a flexible electrodynamic tether. In the first case, the same number of elements are used in the simulated truth data (i.e., simulated dynamic model for which the output is assumed to represent the true state of the system) and the filter predictions. In the second and third cases, different numbers of elements are used to simulate the data and for predicting the tether state. In the final case, the state estimates are used to close the loop using the modified energy-rate feedback controller for flexible electrodynamic tethers.

*Case 1: Truth Model $n = 8$, Filter Model $n = 8$*

In this example, the subsatellite mass is assumed to be 200 kg, the tether length is 10 km, and the total tether mass is 10 kg. The measurement noise covariance is defined by

$$R = \text{diag}[\sigma_{T_x}, \sigma_{T_y}, \sigma_{T_z}, \sigma_{x_1}, \sigma_{y_1}, \sigma_{z_1}]^2$$
$$= \text{diag}[0.25, 0.25, 0.25, 10, 10, 10]^2$$

and the process noise on the kinematic states is $Q = 10^{-5}$, whereas the process noise on the state equations is $10^{-1}$. This level of noise has been selected to take into account systematic modeling errors. The measurement covariances on the tether tip position imply an accuracy of approximately 10 m in all position components. The true initial state of the tether is such that it is aligned with the local vertical. The orbit inclination is 45 deg, and the applied open-loop current is $I = 5 + \sin 2\nu$ A. The initial state covariance is selected as $P_0 = 100Q$. The true initial state is a normally distributed random

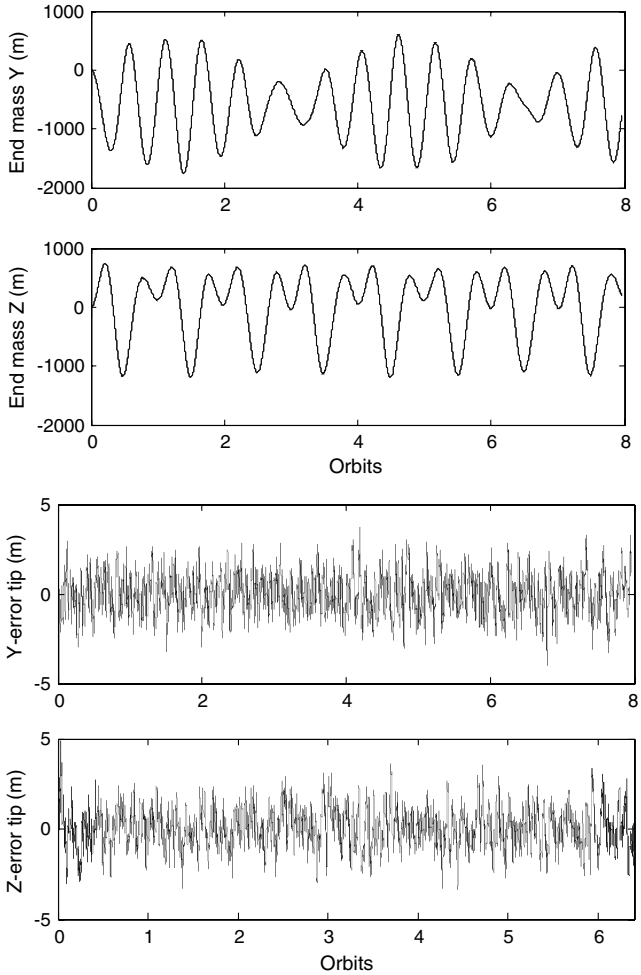


**Fig. 18 State estimates and state-estimation errors of tether tip for flexible electrodynamic tether with same physical model, $n = 8$ (solid lines are estimates and dashes lines are truth).**

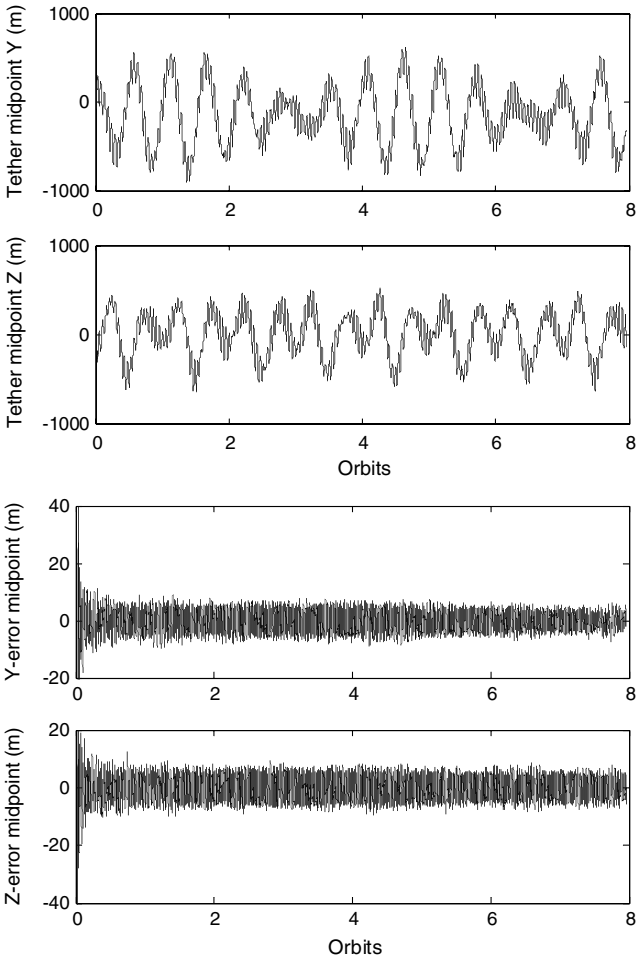


**Fig. 19 State estimates and state-estimation errors for tether midpoint for flexible electrodynamic tether with same physical model, $n = 8$ (solid lines are estimates and dashes lines are truth).**

perturbation to the true state with standard deviation of 0.1 rad (on all state variables). It should be noted that the open-loop current causes the system to become unstable.

Results from the state-estimation process are shown in Figs. 18 and 19 for the case in which the number of discrete masses representing the tether is 8. Figure 18 shows the estimation results for the subsatellite motion. For brevity, only the in-plane and out-of-plane Cartesian coordinates are shown. The longitudinal position of the subsatellite does not give significant insight into the results. It should be noted that the true states are also shown in Fig. 18a, but these are indistinguishable from the state estimates. The results show that the initial error in the state estimates is corrected very quickly by the filter. The is due to the fact that GPS is used for the subsatellite position, which gives much more accurate measurements than using tension only for the subsatellite position. The mean absolute position error of the subsatellite over the final four orbits is 1.34 m. The standard deviation of the error is significantly less than the 10 m accuracy provided by the external reference. Figure 19a shows the state estimates and true states of the tether midpoint (a point not directly measured by any sensor). The results show that the midpoint has substantially higher frequency components than the subsatellite motion, due to the tether flexible modes. Figure 19b shows the state-estimation errors for the midpoint. The mean of the absolute position error taken over the last four orbits is 5.00 m. This represents very good accuracy for a tether 10 km long with measurements taken at the end points only.

*Case 2: Truth Model $n = 8$, Filter Model $n = 4$*

The results in the previous section illustrate that it is possible, with reasonably accurate sensors at the end points, to estimate the tether shape fairly accurately. The limitation of this conclusion is that the mathematical model used to produce the truth and the filter model were the same. The problem is that the real tether will not follow the motion predicted by the discrete tether model. Hence, the degree of discretization required to capture the dynamics reasonably well must be understood. To assess this in a preliminary fashion, the filter is rerun with only four discrete masses representing the tether. The truth data are simulated with eight discrete masses. The filter parameters are the same as the previous case. Numerical results are shown in Fig. 20 for the subsatellite and tether midpoint. Only the estimation errors are shown, due to the fact that the absolute states are virtually indistinguishable on the plot. The results show that the position errors for the subsatellite are larger than in the previous simulated results, despite having identical measurements. The mean of the absolute position error is 2.66 m. Furthermore, the mean of the absolute position error of the tether midpoint (34.54 m) is significantly larger than the previous simulations. Hence, the degree of discretization has a large effect on the resulting state estimates. However, it is not clear whether the larger error is caused by a disparity between the two models or the low number of masses used in the filter model. The following case considers higher-fidelity models of both the truth and filter models.

*Case 3: Truth Model $n = 16$, Filter Model $n = 8$*

In this case, the effect of increasing the fidelity of the truth model relative to the filter model is considered. The truth data are simulated with 16 discrete masses, whereas the filter uses a model with eight discrete masses. The filter parameters and initial conditions are identical to the case 1 data. Results of the state-estimation errors for the subsatellite and midpoint are shown in Fig. 21. These results show that eight discrete masses produce a much more accurate response compared with the 16-mass data than does a four-mass solution with eight-mass data. The mean of the absolute position error of the subsatellite is 1.50 m, which is slightly higher than when

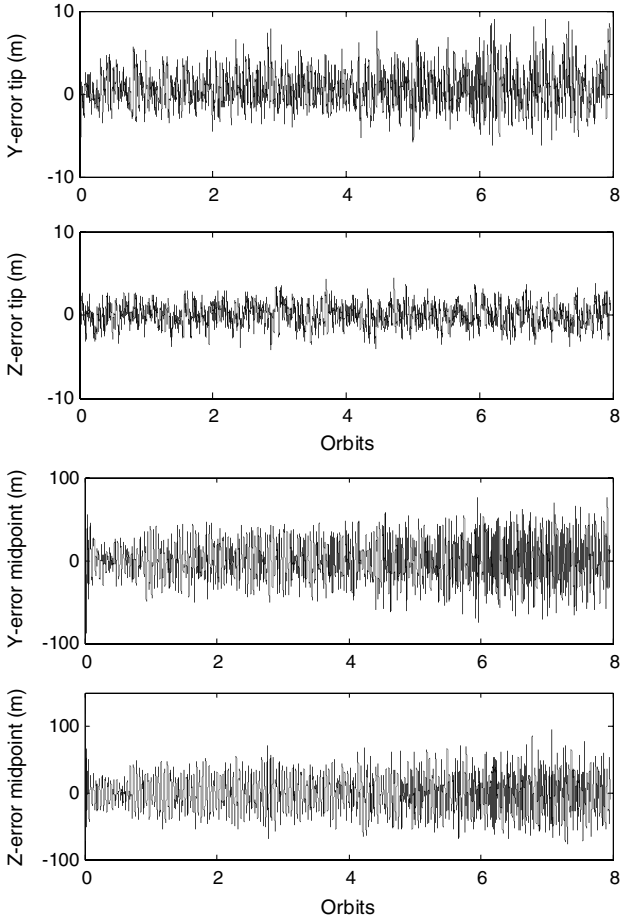


**Fig. 20 State estimation errors for flexible electrodynamic tether with different physical models, $n_{\text{truth}} = 8$ and $n_{\text{filter}} = 4$.**

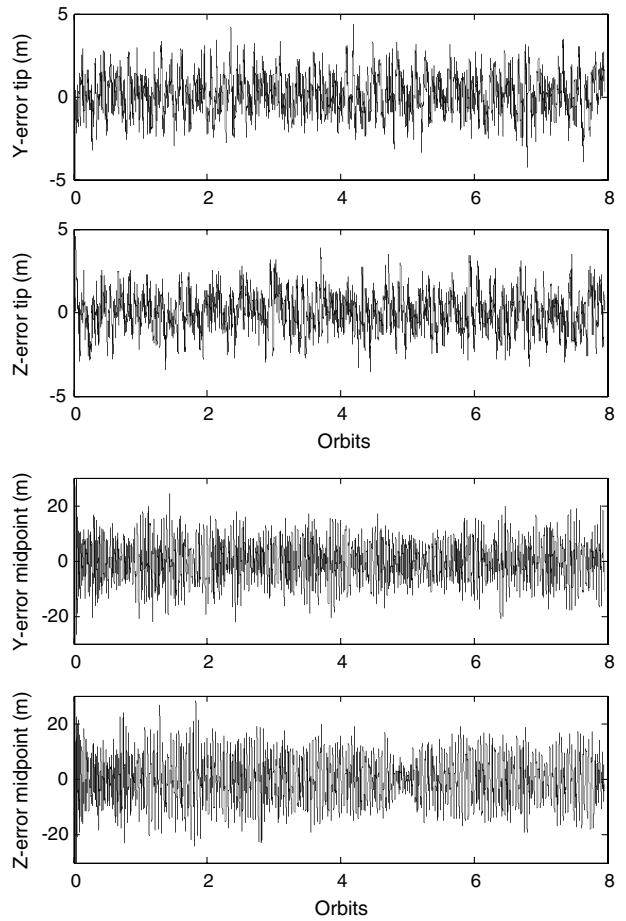


**Fig. 21 State estimation errors for flexible electrodynamic tether with different physical models, $n_{\text{truth}} = 16$ and $n_{\text{filter}} = 8$.**

the same models are used in the filter and truth. The mean of the absolute position error of the tether midpoint is 8.53 m. This suggests that increasing the fidelity of the filter model produces more accurate state estimates relative to the truth. The differences between the models has been assumed to be reflected in the values of the process noise, which may need to be tuned to gain better performance in practice. The difference is also a systematic error that cannot be adequately modeled as a Gaussian error distribution. In such cases, it is often necessary to inflate the process noise to encompass the range of error expected from the disparity of the model with truth. In spite of these issues, the position errors appear to be suitable for implementing feedback controllers for the system. This is considered in the final example shown next.

*Case 4: Feedback Control of Flexible Electrodynamic Using Filtered State Estimates*

In this case, feedback control is applied for stabilizing the flexible electrodynamic tether around the periodic solution using energy-rate feedback. The feedback current is generated using the tether states produced by the filter. In practice, a filter is usually run for a sufficient period of time (or initialized more accurately) to allow it to settle before initializing a feedback controller based on its output. However, in these simulations, the filter and feedback controller are initialized at the same time. Hence, the initial random error applied to the state estimate is used to produce the initial feedback current.

The tether system properties are the same as used in case 1. However, the reference current is selected as $I = 4 + 0.5 \sin 2\nu$ A, i.e., a larger reference current. The reference periodic solution is generated using the method described in Part 1 [19], with $n = 8$. Figure 22a shows the reference periodic solution, and Fig. 22b shows

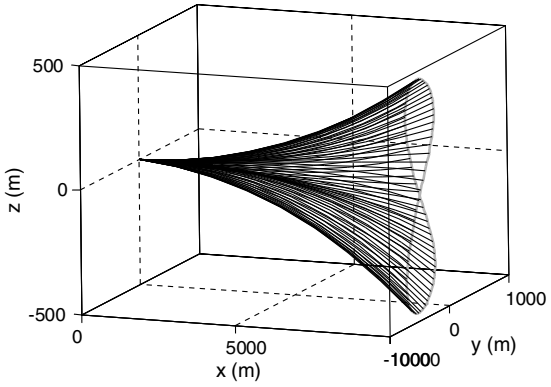


a)

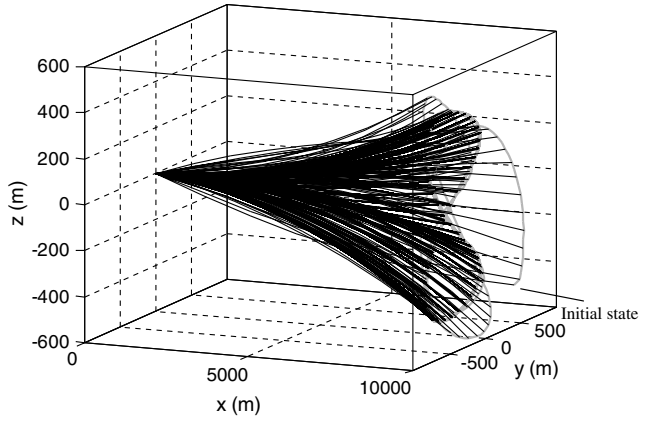


b)

**Fig. 22 Plots of a) reference periodic solution of flexible electrodynamic tether under forced current and b) closed-loop control using filtered states and energy-rate feedback.**

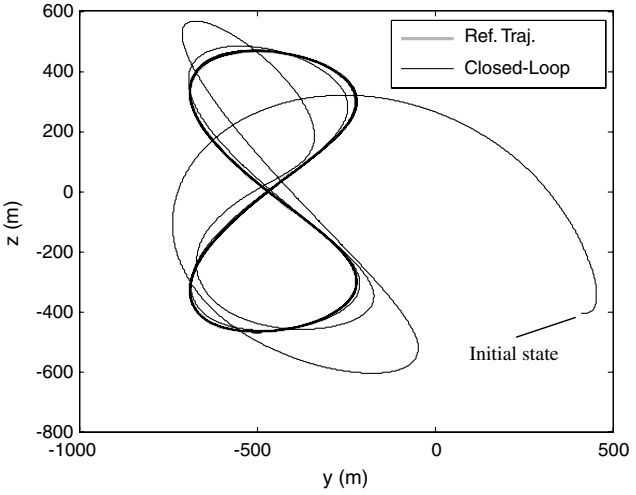


a)

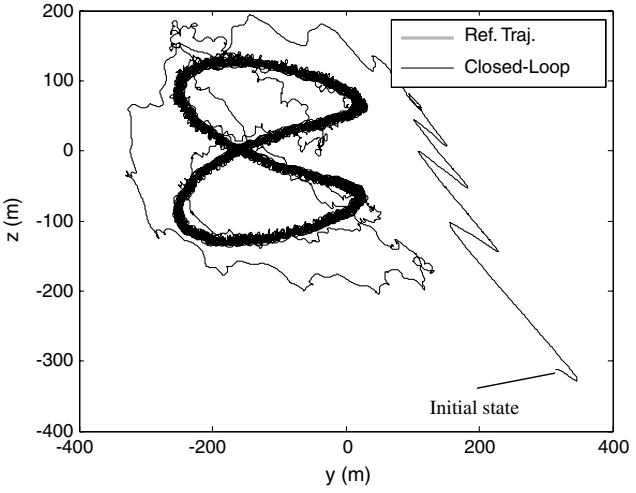


b)

**Fig. 23 Closed-loop trajectory of a) subsatellite and b) tether midpoint.**

the closed-loop trajectory over 15 orbits with a disturbance of 5 deg to the in-plane angle and −5 deg to the out-of-plane angle. Note that the filter model also assumes $n = 8$. The feedback-control gains are selected as $k_2 = 2$ and 1. Figure 22b shows that the entire tether motion is adequately controlled through feedback of the tether current using the filtered states. Figure 23a shows the trajectory of the subsatellite together with the reference trajectory. This clearly illustrates convergence of the trajectory from the relatively large initial error. Furthermore, the initial errors in the state estimates do not appear to have adversely affected the closed-loop behavior of the system. Figure 23b shows the motion of the tether midpoint under closed-loop control. The effects of the imperfect feedback are evident in the lateral tether dynamics, which do not settle to the smooth motion of the reference trajectory. This should also be understood from the point of view that the combined libration and flexible mode control are essentially competing objectives. Too much emphasis on the lateral modes could lead to divergence of the librational motion, and vice versa. Hence, care must be taken when using imperfect states during feedback, as a heavy weighting on the lateral modes could cause a fatal control current to be applied. In this context, the performance of the closed-loop control is very good. Figure 24 shows the state-estimation errors of the subsatellite and tether midpoint. The mean of the absolute position error of the subsatellite is 1.32 m, whereas the mean of the absolute position error of the tether midpoint is 6.53 m. These results are consistent with those presented earlier. Finally, Fig. 25 shows the reference current, together with the

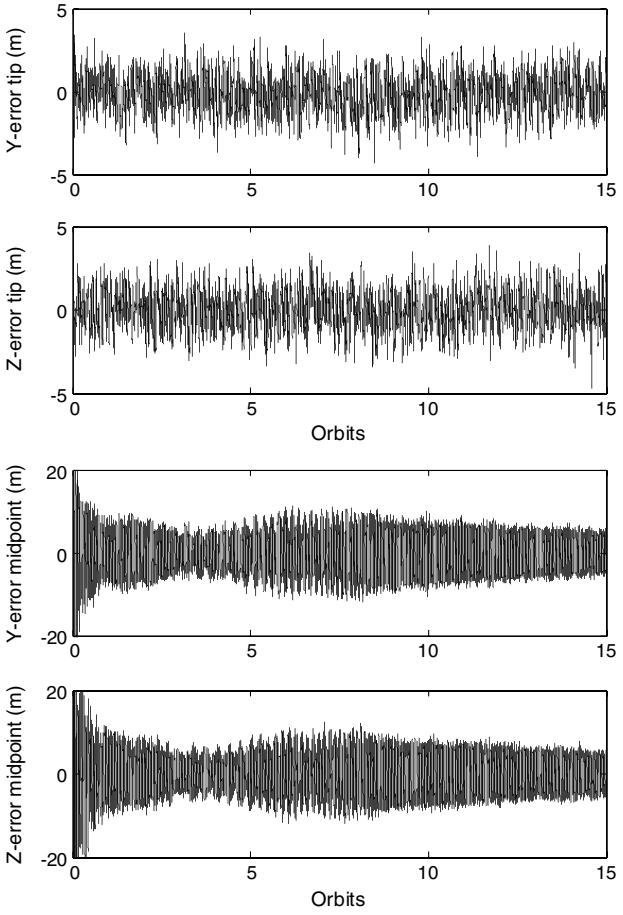


**Fig. 24 State estimation errors for flexible electrodynamic tether during closed-loop control.**

closed-loop current generated for the case of perfect state feedback as well as for filtered state feedback. The initial variation of the current is very similar for the two cases, except that the filtered state feedback produces noisier feedback signals. With perfect state feedback, the current converges to the reference current within approximately three orbits. When filtered estimates are used, the current converges in the mean after roughly six orbits, but it does not converge precisely, due to the fact that the states fed back will never be identical to the true states. Nevertheless, the results clearly demonstrate the applicability of the filtering process and the proposed feedback controller for stabilizing the electrodynamic tether.

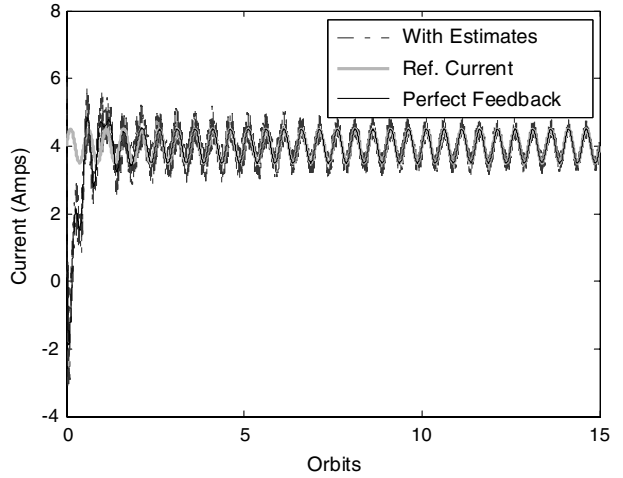


**Fig. 25 Feedback control of tether current during stabilization of flexible electrodynamic tether.**

## Conclusions

The estimation of the relative motion of an electrodynamic tether system using unscented filtering has been studied. Unscented filtering may be used to produce state estimates directly without the tedious derivation of Jacobian matrices that are required by extended Kalman filters. Two cases were considered: libration state estimation using a dumbbell model, and combined libration and shape estimation using a discrete lumped-mass model. The estimates of the tether shape are based on measurements from the end points of the system. Measurement of the tension vector provides information on the dynamic states as well as the orientation of the tether at the main spacecraft. The position of the subsatellite also enables the librational motion to be estimated directly. The ability to accurately estimate the tether shape depends on the accuracy of the sensors as well as on the fidelity of the process model. It was found that the inclusion of eight masses in the discrete model provides a good compromise between filter accuracy and computational demands. An energy-rate feedback controller is able to stabilize the motion of the electrodynamic tether around previously established periodic solutions for both the dumbbell model and the flexible-tether model. Feedback of librations is insufficient to stabilize the complete tether motion when tether flexibility is included. However, the addition of feedback information about the energy present in the lateral dynamics eliminates this problem. The information on energy is obtained using a tension sensor at the main spacecraft. The controller formulated here does not require complete state information and hence can be coupled with a state estimator to produce a more practical controller.

## References

[1] Johnson, L., Estes, R. D., Lorenzini, E. C., Martinez-Sanchez, M., Sanmartin, J., and Vas, I., "Electrodynamic Tethers for Spacecraft Propulsion," AIAA Paper 98-0983, Jan. 1998.

[2] Gallagher, D. L., Johnson, L., Moore, J., and Bagenal, F., "Electrodynamic Tether Propulsion and Power Generation at Jupiter," NASA Marshall Space Flight Center TP-1998-208475, Huntsville, AL, June 1998.

[3] Johnson, L., and Herrmann, M., "International Space Station Electrodynamic Tether Reboost Study," NASA Marshall Space Flight Center/TM-1998-208538, July 1998.

[4] Tragesser, S. G., and San, H., "Orbital Maneuvering with Electrodynamic Tethers," *Journal of Guidance, Control, and Dynamics*, Vol. 26, No. 5, 2003, pp. 805–810. doi:10.2514/2.5115

[5] Williams, P., "Simple Approach to Orbital Control Using Spinning Electrodynamic Tethers," *Journal of Spacecraft and Rockets*, Vol. 43, No. 1, 2006, pp. 253–256. doi:10.2514/1.16608

[6] Williams, P., Blanksby, C., and Trivailo, P., "The Use of Electromagnetic Lorentz Forces as a Tether Control Actuator," *52nd International Astronautical Congress*, International Astronautical Federation, Paper IAC 02-A.5.04, Oct. 2002.

[7] Tani, J., and Qiu, J., "Motion Control of a Tethered Subsatellite Using Electromagnetic Force," *Proceedings of the Seventh International Conference on Adaptive Structures*, Technomic, Lancaster, PA, Sept. 1997, pp. 321–330.

[8] Williams, P., Watanabe, T., Blanksby, C., Trivailo, P., and Fujii, H. A., "Libration Control of Flexible Tethers Using Electromagnetic Forces and Movable Attachment," *Journal of Guidance, Control, and Dynamics*, Vol. 27, No. 5, 2004, pp. 882–897. doi:10.2514/1.1895

[9] Takeichi, N., "Libration Control of an Electrodynamic Tethered System through Electric Current Switching," *AAS/AIAA Astrodynamics Specialists Conference*, Lake Tahoe, NV, American Astronautical Society Paper 05-318, Aug. 2005.

[10] Peláez, J., and Lorenzini, E. C., "Libration Control of Electrodynamic Tethers in Inclined Orbit," *Journal of Guidance, Control, and Dynamics*, Vol. 28, No. 2, 2005, pp. 269–279. doi:10.2514/1.6473

[11] Williams, P., "Energy Rate Feedback for Libration Control of Electrodynamic Tethers," *Journal of Guidance, Control, and Dynamics*, Vol. 29, No. 1, 2006, pp. 221–223. doi:10.2514/1.17530

[12] Inarrea, M., and Peláez, J., "Libration Control of Electrodynamic Tethers Using the Extended Time-Delayed Autosynchronization Method," American Astronautical Society Paper 07-194, Jan. 2007.

[13] Williams, P., "Libration Control of Electrodynamic Tethers using Predictive Control with Time-Delayed Feedback," *Journal of Guidance, Control, and Dynamics*, Vol. 32, No. 4, 2009, pp. 1254–1268.
doi:10.2514/1.41039

[14] Peláez, J., Lorenzini, E. C., Lopez-Rebollal, O., and Ruiz, M., "A New Kind of Dynamic Instability in Electrodynamic Tethers," American Astronautical Society, Paper AAS 00-190, 2000.

[15] Peláez, J., and Lara, M., "Periodic Solutions in Electrodynamic Tethers on Inclined Orbits," *Journal of Guidance, Control, and Dynamics*, Vol. 26, No. 3, 2003, pp. 395–406.
doi:10.2514/2.5077

[16] Peláez, J., Ruiz, M., Lopez-Rebollal, O., Lorenzini, E. C., and Cosmo, M. L., "Two-Bar Model for the Dynamics and Stability of Electrodynamic Tethers," *Journal of Guidance, Control, and Dynamics*, Vol. 25, No. 6, 2002, pp. 1125–1135.
doi:10.2514/2.4992

[17] Peláez, J., and Andres, Y. N., "Dynamic Stability of Electrodynamic Tethers in Inclined Elliptical Orbits," *Journal of Guidance, Control, and Dynamics*, Vol. 28, No. 4, 2005, pp. 611–622.
doi:10.2514/1.6685

[18] Hoyt, R. P., "Stabilization of Electrodynamic Space Tethers," *Proceedings of Space Technology and Applications International Forum (STAIF-2002)*, American Inst. Of Physics, Melville, NY, 2002, pp. 570–677.

[19] Williams, P., "Electrodynamic Tethers Under Forced Current Variations Part 1: Periodic Solutions for Tether Librations," *Journal of Spacecraft and Rockets*, Vol. 42, No. 2, 2009, pp. 308–319.
doi:10.2514/1.45731

[20] Williams, P., "Direct Numerical Computation of Periodic Orbits and Their Stability," *Journal of Spacecraft and Rockets*, Vol. 43, No. 5, 2006, pp. 1143–1146.
doi:10.2514/1.20930

[21] Ruiz, M., Lopez-Rebollal, O., Lorenzini, E. C., and Peláez, J., "Modal Analysis of the Stability of Periodic Solutions in Electrodynamic Tethers," *Astrodynamics 2001*, Advances in the Astronautical Sciences, Vol. 109, Univelt, San Diego, CA, 2001, pp. 1553–1570.

[22] Williams, P., "Deployment/Retrieval Optimization for Flexible Tethered Satellite Systems," *Nonlinear Dynamics*, Vol. 52, Nos. 1–2, 2008, pp. 159–179.
doi:10.1007/s11071-007-9269-3

[23] Williams, P., Hyslop, A., Stelzer, M., and Kruijff, M., "YES2 Optimal Trajectories in Presence of Eccentricity and Aerodynamic Drag," *Acta Astronautica*, Vol. 64, Nos. 7–8, 2009, pp. 745–769.
doi:10.1016/j.actaastro.2008.11.007

[24] Julier, S. J., Uhlmann, J. K., and Durrant-Whyte, H., "A New Approach for Filtering Nonlinear Systems," *Proceedings of the American Control Conference*, Inst. of Electrical and Electronics Engineers, Piscataway, NJ, 1995, pp. 1628–1632.

[25] van der Merwe, R., and Wan, E. A., "The Square-Root Unscented Kalman Filter for State and Parameter-Estimation," *Proceedings of International Conference on Acoustics, Speech, and Signal Processing*, Inst. of Electrical and Electronics Engineers, Piscataway, NJ, May 2001, pp. 3461–3464.

C. Kluever
*Associate Editor*